Localized Co-delivery of Serca2a and Cx43 Genes Combined With Bone Marrow Mesenchymal Stem Cells Restores Rat Ischemic Cardiac Mechano-electrical Function

Wei Wang
Xinjiang Medical University Affiliated First Hospital
Baihetiya Tayier
Xinjiang Medical University Affiliated First Hospital
Lina Guan
Xinjiang Medical University Affiliated First Hospital
Fei Yan
Shenzhen Institutes of Advanced Technology Chinese Academy of Sciences
Yuming Mu (mym1234@126.com)
Xinjiang Medical University Affiliated First Hospital

Research

Keywords: Ca2+-ATPase 2a, Connexin 43, Myocardial infarction, Gene delivery, Biotinylated microbubbles

Posted Date: November 13th, 2020

DOI: https://doi.org/10.21203/rs.3.rs-105302/v1

Abstract

Aim: Significantly reduced expression of Ca^{2+}-ATPase 2a (SERCA2a) and Connexin 43 (Cx43) which play important roles in regulating mechano-electrical function was found in an ischemic heart. Bone marrow mesenchymal stem cells (BMSCs) transplantation brings with a weak improvement of ischemic heart in cardiac contractility and anti-arrhythmias effect. The aim of this study was to recover mechano-electrical function of ischemic heart through combining stem cell therapy with SERCA2a/Cx43 co-delivery by biotinylated microbubbles (BMBs) via ultrasound targeted microbubble destruction (UTMD).

Methods: Dual gene-loaded BMBs were developed through conjugating SERCA2a-adenovirous (S-Ad) and Cx43-adenovious (C-Ad) onto BMBs via biotin-avidin linkage. UTMD was used to mediate the local co-delivery of S-Ad and C-Ad into the infarct zone where BMSCs were transplanted. The expression of SERCA2a and Cx43 gene, neovascularization in the infarct area and mechano-electrical function of rats were detected.

Results: UTMD-mediated dual gene delivery could significantly enhance the expression of SERCA2a/Cx43 genes in the infarct zone receiving BMSCs transplantation. Significantly improved neovascularization was observed. More importantly, UTMD-mediated dual gene delivery greatly improved cardiac function and reduced arrhythmia in these myocardial infarct (MI) hearts transplanted with BMSCs.

Conclusions: BMSCs-based dual gene therapy can effectively improve cardiac mechano-electrical function and reduce arrhythmia in heart with MI. It is necessary to rebuild the gene network in damaged heart rather than supply a single gene. BMSCs transplantation combined with localized dual-gene delivery by UTMD might point out a novel strategy to recover mechano-electrical function of ischemic heart.

Introduction

Ischemic heart disease is a significant cause of morbidity and mortality worldwide [1]. Transplantation with bone marrow mesenchymal stem cells (BMSCs) is considered as an ideal approach in myocardial infarction (MI) therapy due to their advantages as follows: 1) MSCs can secrete some growth factors, such as vascular endothelial growth factor (VEGF) and stromal cell derived factor 1 (SDF-1), to elevate angiogenesis or to promote the formation of novel vasoganglion via paracrine effect [2]. 2) BMSCs are capable to inhibit the production of active inflammatory factors and improve the inflammatory microenvironment or directly regulating the functions of immune cells after MI [3,4]. 3) BMSCs can prevent cardiac fibrosis by releasing hepatocyte growth factor (HGF), and thus reverse LV remodeling and restore the cardiac function [5]. 4) BMSCs can home to the infarction area after transplantation with the help of SDF-1 and its receptor CXC chemokine receptor 4 (CXCR4). 5) BMSCs have the capacity for multidirectional differentiation, contributing to the regeneration of the vasculature after MI [6]. Despite all of the benefits brought by MSCs, this approach only shows a faint efficacy in restoring cardiac contractility and preventing ischemia-induced arrhythmias after MI. The main reason which causes

unsatisfactory efficacy may attribute to the abnormal Ca^{2+} handling accompanied by undermined cell-cell coupling within infarct and peri-infarct region.

It has been well established that myocardial ischemic stress strongly modifies the profile of gene expression in heart [7] including sarcoplasmic reticulum Ca^{2+}-ATPase 2a (SERCA2a) and Connexin 43 (Cx43), two key proteins that regulate mechano-electrical function [8,9]. SERCA2a governs the intracellular Ca^{2+} handling process [10], by which cardiac contraction and relaxation is maintained through mediating Ca^{2+} reuptake into sarcoplasmic reticulum (SR) [11]. A reduced SERCA2a level or impaired function will result in the overload of intracellular Ca^{2+} and utterly myocardial dysfunction after MI [12]. Cx43 is another significantly decreased protein which takes vital role in the gap junctions (GJs) of myocardial cells in ischemic myocardial tissue. GJs mediate electrical coupling between cardiac myocytes, forming the cell-to-cell pathways for orderly spread of the wave of electrical excitation responsible for synchronous contraction, and the impaired electrical coupling could consequence in increased inclination for arrhythmias [13]. GJs channel is consisted of six transmembrane proteins in atrial and ventricular myocytes and Cx43 is the most abundant member among them. Previous studies have demonstrated that the reduced Cx43 expression and its abnormal distribution eventually result in arrhythmias [14]. In this context, it is necessary to enhance the expression levels of SERCA2a and Cx43 genes in the recovery of cardiac function, especially during the transplantation treatment with stem cells after MI.

Recent years, gene therapy has drawn great attention due to its favorable therapeutic benefits in the treatment of various diseases [15], including tumors [16], cardiac diseases [17] and nervous system disorders [18]. However, it remains a grand challenge to selectively and effectively deliver the genes into targeted cells with minimal side-effect. To date, various virus gene delivery vectors or vehicles, such as adenovirus (Ad), lentivirus and adeno associated virus (AAV), provide an approach with high gene transfection efficiency, but lack of specific tissue or organ targeting capability for these virus vectors limit their clinical applications to some extent [19]. Thus, there is great demand to develop a strategy to help these viral vectors to locally deliver into target tissues. More recently, ultrasound-targeted microbubble destruction (UTMD) has been proved a promising approach for local delivery of genes or drugs [20-22]. Ultrasound beams transmitted by a focused transducer can penetrate soft tissues and be focused into a special organ such as a heart. When there are microbubbles (MBs) in the blood vessels, the ultrasound energy in the focused site will induce the bubble resonance, producing a series of acoustic cavitation effects, including stable cavitation and inertial cavitation. The former induces microstreaming in the flow of liquid around the MBs that brings with shear stress to cell membranes due to the repetitive MB contraction and expansions. The latter causes abrupt MB destruction to produce stronger mechanical stress, such as shock waves, microjets, etc. These acoustic cavitation effects collectively cause cell membrane perforation and locally enhance blood vessel permeabilization [23].

In this study, taking the great advantages of high virus gene transfection efficiency and localized gene delivery by UTMD, we attempt to combine stem cell-based strategy and gene therapy to improve the

efficacy in the restoration of mechano-electrical function after MI (Abstract graphic). Briefly, Ad-loaded MBs were firstly constructed through coating the SERCA2a-Ad (S-Ad) and Cx43-Ad (C-Ad) onto the surface of MBs via a biotin-avidin linkage. After being intravenously injected into the MI rats transplanted with BMSCs, ultrasound irradiation was applied to release and deliver the Ads locally into the infarct myocardial tissues. SERCA2a and Cx43 overexpression will accelerate neovascularization in infarct zone and present better restoration in mechano-electrical function than cell-based method alone.

Methods

Fabrication of gene loaded biotinylated microbubbles and gene-loaded BMBs

Biotinylated microbubbles (BMBs) carrying FITC-labeled SERCA2a/GFP-encoded Ad (named as S-BMBs), BMBs carrying rhodamine-labeled Cx43/RFP-encoded Ad (C-BMBs) and BMBs carrying both Ads (S/C-BMBs) as previously described [24]. Briefly, DSPC, DSPE-PEG2000 and DSPE-PEG2000-Biotin (molar ratios = 9:0.5:0.5) were dissolved in chloroform. The solvent was then evaporated under nitrogen flow at room temperature, producing a thin layer of phospholipid membrane. After two-hour vacuum treatment, the completely dried phospholipid membrane was hydrated at 60 °C with Tris (hydroxymethyl) aminomethane buffer saline, and transferred into vials (1 mL for each). After sealing the vials, perfluoropropane (Flura, Newport, TN, USA) was added. These vials with phospholipid suspension were mechanically vibrated for 30 s. The resulting BMBs were rinsed and incubated with streptavidin. After eliminating free streptavidin by PBS rinse, these BMBs (about 1×10^9) were further incubated with Ad to fabricate the gene-loaded BMBs.

Characterization of BMBs and gene-loaded BMBs

Particle size and size distribution of MBs were measured with Accusizer 780 Optical Particle Sizer (Particle Sizing Systems, Santa Barbara, CA, USA). A drop (about 20 μL) of each kind of BMBs suspension was applied to the microscope slide and observed under an optical microscope (Olympus, Tokyo, Japan). Furthermore, each kind of BMBs suspension was negatively stained with an aqueous solution of uranyl acetate and observed using a transmission electron microscope.

BMBs stability

The stability of BMBs was manifested by the change in the particle size and concentration over time. The particle size and concentration of 1ml of diluted BMBs were measured immediately after the completion of fabrication at room temperature, or after 15, 30, 45 and 60 mins by Accusizer 780 Optical Particle Sizer.

Gene loading capacity of BMBs

To determine the gene loading capacity of BMBs, FITC-labeled SERCA2a/GFP-encoded adenovirus (S-Ad) or rhodamine-labeled Cx43/RFP-encoded adenovirus (C-Ad) range from 1.25 μl to 20 μl (1×10^9 pfu/ml)

was mixed with BMBs to fabricate gene loaded BMBs (S-BMBs or C-BMBs), respectively. Then, the gene loading capacity was determined by flow cytometry and qPCR. After determined the lowest amount of Ad to achieve the maximum gene loading efficiency. Furthermore, S-Ad and C-Ad was added into BMBs to making dual gene-loaded BMBs (S/C-BMBs) at the ratio of 1:1, 1:2 or 2:1, respectively. Next the dual gene loading capacity was determined by flow cytometry and qPCR.

Isolation culture and identification of BMSCs

Conforming to the Directive 2010/63/EU of the European Parliament, SD (Sprague Dawley) rats at 4 weeks of age were euthanatized with pentobarbital sodium (60 mg/kg body weight, Sigma-Aldrich Inc., USA) via intraperitoneal injection once. Then, bilateral tibial and femoral bones were dissected from body trunk and stored on ice in 75% alcohol. Subsequently, femurs and tibias were separated and both ends of each femur or tibia were cut, and a 22-gauge needle attached to a 10cc syringe containing complete medium was then inserted into the spongy bone exposed by removal of the growth plate. The marrow plug is then flushed from the bone with 5 ml of complete medium and collected in a 50 ml conical tube. Cells were then cultured in T-75 cell culture flask, with a cell concentration of 1×10^5/mL, using Mouse Mesenchymal Stem Cell Growth Medium (Cyagen, China). BMSCs were then purified and passaged by attachment method. Cells were incubated under standard cell culture conditions with 5% CO_2, at 37 °C and 95% relative humidity. The medium was changed every three days, and BMSCs were passaged when 80%-90% confluence was reached. BMSC identity was confirmed on the basis of morphological criteria, plastic adherence, and specific surface antigen expression: CD29(+), CD90(+), CD45(−).

Ultrasound-mediated gene transfection with BMBs *in vitro*

Ultrasound-mediated gene transfection was performed by using an ultrasound system including an arbitrary waveform generator (model AFG3102, Tektronix, USA), an RF power amplifier (model AR150A100B, AR, USA), and a single-element planar ultrasound (US) transducer (frequency = 1 MHz; Valpey Fisher Corp., MA, USA). Briefly, BMSCs were seeded in 12-well plates (1×10^5 cells per well) and transfection experiments were conducted when the cell confluence reached 70–80%. Then gene-loaded BMBs were added to the well, and to guarantee a close contact between transfection complexes and cells, the 12-well plate was sealed firmly and inverted for 15 min. Then ultrasound exposure was performed. The multiplicity of infection (MOI) was adjusted to 500 throughout the study. Ultrasound conditions were set as follows: frequency 1 MHz, power 2.0 W/cm^2, duration 60 s, duty cycle 10%.

Detection of the *in vitro* gene transfection efficiency

To examine the ultrasound-mediated gene transfection efficiency, the following groups were included: (1) Control group; (2) Ad group, only Ad was used to transfect BMSCs; (3) Ad + US group, Ad was used to transfect BMSCs under the aid of ultrasound; (4) Ad + UTMD group, gene-loaded BMBs was use to transfect BMSCs under the aid of ultrasound. These BMSCs were cultured for another 48 h. Fluorescence microscopy was applied to detect GFP and RFP expression of each group, western blot and qPCR analysis to detect SERCA2a and Cx43 protein and mRNA level of each group.

Cell viability assay and *in vivo* biocompatibility

Cell viability was measured immediately after the gene transfection using a Cell Counting Kit-8 (CCK-8) according to the manufacturer's protocol (Dojindo, Japan) to determine the possible cell damage caused by UTMD. Relative cell viability (RCV) was assessed using CCK-8 assay and then determined in a 96-well plate reader (BioTek Synergy 4) at 450 nm wavelength with the equation RCV (%) = At − Anc/Apc − Anc ×100%. Furthermore, to evaluate the *in vivo* biocompatibility of the BMBs, healthy SD rats were intravenously injected with gene-loaded BMBs. On the 15^{th} day post-injection, fresh blood samples (1.0 mL) were obtained by cardiac puncture from the rats for serum biochemistry study. Subsequently, the major organs including lungs liver, spleen and kidneys of were carefully collected for H&E staining histology analysis. Healthy rats without any intervention were used as the control.

Animal model

The experimental protocol was approved by the Animal Ethics Committee of the First Affiliated Hospital of Xinjiang Medical University (approval number of IACUC-20160218-057). Following the ARRIVE criteria [25], the experiment was carried out in strict accordance with the "3R" principle of substitution, reduction and optimization to minimize damage to animals. Male or female healthy SD rats (8~10 weeks old, weight 200-260 g) were purchased from Beijing Vital River Laboratory Animal Technology Co., Ltd. The experimental animals were well housed under standard conditions of room temperature and dark-light cycles with sufficient water and food.

On the first day of the experiment, rats were induced for anesthesia with Dexmedetomidine (0.3 mg/kg body weight, Sigma-Aldrich Inc., USA)/midazolam (4.0 mg/kg bw, Sigma-Aldrich Inc., USA)/butorphanol (5.0 mg/kg bw, Sigma-Aldrich Inc., USA) [26] via intraperitoneal injection once. Then, the rats were intubated with a 16G intravenous catheter (Introcan 16G, Braun Medical Co., Ltd., Germany) and ventilated with a rodent ventilator (HX-100E, Taimeng Software Co., Ltd., Chengdu, China). Left anterior descending artery (LAD) ligation was performed as previously described [27]. The rat's heart was fully exposed by thoracotomy. Finding the coronary vein as a landmark, then permanently ligated the LAD approximately 2~3 mm distal from its origin with a depth of 0.5 mm by a 5/0 suture. Evidence of a MI was confirmed by pale and hypokinesia in the left ventricular anterior wall and ST-segment elevation on an electrocardiogram. Penicillin 160,000 u was intraperitoneal injected for 3 days after the surgery.

Experimental animal groups

Forty-eight successfully modeled SD rats were randomly divided into control and experimental groups: (1) Control group (MI + PBS, n = 8); (2) UTMD group (MI + PBS + US-BMBs, n = 8); (3) BMSCs group (MI + BMSCs, n = 8); (4) B+S+U group (MI + BMSCs + US-S-BMBs group, n = 8); (5) B+C+U group (MI + BMSCs + US-C-BMBs group, n = 8); (6) B+S/C+U group (MI + BMSCs + US-S/C-BMBs-1:1 group, n = 8). Another 8 randomly chosen healthy rats were operated without ligation and divided into SHAM groups.

BMSCs transplantation

Four weeks after the successful ligation, the rats underwent surgery again. The rats from SHAM, Control and UTMD groups were injected with PBS (100 μl). Rats from the rest groups were injected with BMSCs (5×10^6, 100 μl) at the myocardial infarct zone and the peri-infarct zone.

UTMD-mediated localized co-delivery of genes

Two days after BMSCs transplantation [20], UTMD-mediated gene localized co-delivery was performed. The treatment groups were infused with 100 μl of the S-BMBs, C-BMBs or S/C-BMBs respectively via the tail vein at a constant rate (15 ml/h), and then washed with PBS 100 μl. A Mindray Kunlun 7 ultrasound machine with a line array probe (L 11-3 U) was used at a setting of fundamental frequency 5.6 MHz-11.8 MHz, harmonic frequency 7 MHz ~ 9 MHz and mechanical index 0.53. Contrast mode was activated at the beginning of infusion. On seeing the filling of BMBs in the left ventricle cavity, the FLASH (mechanical index: 1[20]) function was triggered manually at an interval of 3 s ~ 5 s, lasting for 10 mins [28]. The rats of Control group were infused with PBS 100 μl and performed as above.

Left ventricular function analyzing

Echocardiography was performed 4 weeks after AMI and 2 weeks and 4 weeks post-treatment. A Vevo2100® ultrasound imaging system (High-Resolution Micro-Imaging System, VisualSonics, Canada) equipped with an 18 MHz transducer was used by an investigator blinded to group designation. The left ventricular ejection fraction (LVEF) and left ventricular fractional shortening (LVFS) were calculated by M-mode tracing. The dimension data are presented as the average of measurements of three selected beats.

Electrophysiological examination

Steady-state pacing was performed to test the ability of anti-arrhythmia after treatment. On the 28^{th} day after BMSCs transplantation, Rats were induced for anesthesia by intraperitoneal injection of sodium pentobarbital (30 mg/kg body weight, Sigma-Aldrich Inc., USA) once. ECG monitoring (BL-420F biological function experiment system, Taimeng Software Co., Ltd., Chengdu, China) was used to record the ECG activity in real time. The stimulation protocol was performed as described previously [29]. Briefly, the left chest was opened to fully expose the heart after anesthesia. A bipolar pacing electrode was placed in the left ventricular wall near the apex of the heart, with a diameter of 0.2 mm and a distance of 3 mm between the two electrodes. Continuous progressive stimulation (S1S1) was given to induce ventricular arrhythmias. Stimulus plan is that as below, pulse width of 0.1ms, step length at -2 ms, stimulus frequency starts at 5 Hz and stimulus voltage begins with 5 V, gradually increasing by 1 V. End point of stimulation is induction of ventricular tachycardia (VT) or ventricular fibrillation (VF) with more than 6 consecutive ventricular premature beats. After the Electrophysiological examination, the rats were euthanized by pentobarbital sodium (60 mg/kg body weight, Sigma-Aldrich Inc., USA) [26] via intraperitoneal injection once, and the hearts were taken for subsequent test. The procedure conformed to the Directive 2010/63/EU of the European Parliament.

Enzyme-linked immunosorbent assay (ELISA) analysis

ELISA was applied to determine the levels of SERCA2a and Cx43 in the infarcted myocardial tissue homogenates. commercial ELISA kits (R&D systems) were used per the manufacturer's instructions. Samples and standards were prepared according to manufacturer's instructions.

Western blot assay

Protein expression levels of SERCA2a, Cx43, VEGF and cardiac-specific proteins (cTnT and α-actin) in the infarct zone were detected by Western blot according to the previous study. [30] Total proteins were extracted from treated myocardial infarct tissue using a RIPA buffer with protease and phosphatase inhibitors (G2002, Wuhan Servicebio Co., Ltd., China). The protein concentrations were determined by the Bicinchoninic acid (BCA) method as a protein standard. Proteins were separated by electrophoresis, transferred to a cellulose acetate membrane and blocked. The primary antibody (GB23303, Wuhan Servicebio Co., Ltd., China) was added followed by the secondary antibody (GB23302, Wuhan Servicebio Co., Ltd., China). The density of each band was quantitated by a densitometer with AlphaView Software for FluorChem Systems (ProteinSimpleTM).

Analysis of immunofluorescent protein expression

Immunofluorescence was performed to detect SERCA2a and Cx43 protein expression in the infarcted myocardium. Frozen sections of myocardial tissue were prepared as described previously [31]. Then, the prepared frozen sections were incubated with 5% (volume fraction) bovine serum albumin (Solarbio, China) for 30 mins. The primary antibody (at 1:100 /1:200 volume) was added, incubated overnight at 4 ℃, and then washed thrice for 5 mins with PBS. Next, the fluorescently labeled secondary antibody (at 1:300/1:400 volume) was added and incubated at 37 ℃ for 50 min. The slides were washed as above. Subsequently, the image was observed and photographed using a fluorescence microscope (Nikon Eclipse TI-SR, Nikon Inc., Japan). The fluorescence area ratio was quantitated with Image-Pro Plus version 6.0 software (Media Cybernetics, Bethesda, MD) by 2 observers blinded to the conditions.

Histological evaluation of neovascularization in the infarcted zone

To evaluate neovascularization, formaldehyde-fixed rat hearts were dehydrated and then embedded in paraffin. Paraffin-embedded sections (4 μm) were dewaxed and incubated with the primary antibody against factor VIII (ThermoFisher Scientific, America). After visualization with diaminobenzidine (DAB), we counted the positively stained micro-vessels under a Nikon eclipse E100 light microscope (Nikon Inc., Japan; 100× magnification). Microvascular endothelial cells showed a layer of brown ring-like precipitates with a diameter of less than 20 μm, which were calculated as previously described [32]. All histological analyses were independently performed by two experienced pathologists under double-blinded conditions.

Measurement of the infarct size

Twenty eighty days after treatment, the rats were euthanasized with overdose of pentobarbital sodium (60 mg/kg body weight, Sigma-Aldrich Inc., USA) via intraperitoneal injection once. Then, after cardiac perfusion with saline hearts of the rats were extracted and fixed in 4% paraformaldehyde (Wei Bio Technology Co., Ltd., Shanghai, China). Paraffin-embedded samples were sectioned at 4 μm, and Masson's trichrome staining was performed. The infarcted zone was evaluated based on the percentage of blue staining, indicative of fibrosis, and quantitated with Image-Pro Plus version 6.0 software by two observers blinded to the conditions.

Statistical analysis

All data are summarized as mean ± standard deviation. The data were analyzed using SPSS 21.0. Parametric comparisons were tested by One-way analyses of variance (ANOVA) with subsequent post-hoc multiple comparisons using the least significant difference (LSD) test. Probability values $P < 0.05$ were considered statistically significant.

Results

Fabrication and characterization of biotinylated microbubbles (BMBs)

The fabrication process of BMBs was illustrated in Fig. 1a. Briefly, the mixture of DSPC, DSPE-PEG2000, DSPE-PEG-Biotin dissolved in chloroform was applied to form the lipid shell of BMBs and C_3F_8 was used as the gas core (for sample preparation details, see Methods). The resulting BMBs were firstly coated with streptavidin, followed by incubation with Ad particles, leading to the production of Ad-BMBs. The lipid solution was transparency liquid (Fig. 1b left), BMBs appeared milky after oscillation (Fig. 1b right). Fig. 1F presents the microscopic image of BMBs, showing a bright gas core surrounded by dark circular rings. Then scanning electronic microscopy (SEM) was performed to further determine the morphology of these bubbles (Fig.1c). Fig. 1d presented the particle size distribution of the BMBs, showing average particle size of 1.10 ± 0.65 μm with a polydispersity index (PDI) of 0.26 ± 0.05. The freshly fabricated BMBs had a concentration of $4.63 \pm 0.62 \times 10^9$ bubbles/ml as shown in Table 1. Considering that the Ad loading process takes approximately 40 mins, the BMBs must keep stable during this period of time. Fig. 1e revealed that the mean diameter did not show any difference during 60 mins and the bubble concentration stayed the same after 40 mins, proving that the self-assembled BMBs possessed a desirable stability. The ultrasound images of BMBs showed sufficient contrast signals detected by ultrasound *in vitro* and *in viv*o (Fig. S1). Thus, BMBs were successfully fabricated.

Formation of Ad-BMBs and Ad loading capacity of BMBs

FITC-labeled S-Ad, Rhodamine-labeled C-Ad or both were further loaded onto the surface of BMBs via biotin-streptavidin linkage. As presented by the bright-field and corresponding fluorescent images (Fig. 1f), these bubbles emitted the green or red fluorescence onto the surface of BMBs, showing FITC-labeled S-Ad or Rhodamine-labeled C-Ad were successfully loaded onto the surface of BMBs. The loading ratio was further confirmed by flow cytometry and qPCR. Fig. 1g demonstrated that the positive ratio increased

along with the increasing dose of Ad (BMBs were kept at 1×10^9 bubbles/ml) and then reached saturation with 92.57±3.61% for S-BMBs and 92.47±3.54% for C-BMBs, respectively by flow cytometry. Also, data from qPCR (Fig. 1h) showed that gene-loading ratio reaches the maximum ((91.59±1.04% for S-Ad, 90.72±1.69% for C-Ad when adding 10 μl Ad (1×10p pfu/ml) to BMBs (100 μl, 1×10^9/ml)), revealing that 1×10^8 BMBs could bind approximately 1×10^7 pfu of Ad. To determine both S-Ad and C-Ad loading capacity of BMBs (S/C-BMBs), both S-Ad and C-Ad were incubated with BMBs (100 μl, 1×10^9 bubbles/ml) at the ratio of 1:1 (10 μl : 10 μl), 1:2 (5 μl : 10 μl) or 2:1 (10 μl : 5 μl), respectively. Fig. 1i demonstrate a similar Ad loading ratios for S-Ad (66.77±1.11%, green) and C-Ad (65.62±1.01%, red) at the ratio of 1:1, while S-Ad or C-Ad was dominant at the ratio of 2:1 or 1:2, respectively (Fig. 1j), indicating an inspiring result that the dual gene-loaded BMBs could achieved a satisfying Ad loading efficiency at the ratio of 1:1.

In vitro UTMD-mediated gene transfection

To confirm the UTMD-mediated gene transfection efficiency *in vitro*, BMSCs were cultivated (Fig. S2a) and identified (Fig. S2b), then were seeded in 24-well plates and divided into four groups: (1) control group without any intervention; (2) Ad only group; (3) Ad + US group, and (4) Ad + UTMD group. A fluorescence microscope was used to detect the expression of GFP or RFP at 48 h after application of S-Ad or C-Ad. As presented in Fig. 2a, GFP expression displayed a burst elevation in Ad group comparing to the control which did not show any fluorescence signals. Strikingly, the GFP positive cells can be increased with the aid of UTMD, while US alone could not bring any benefit to Ad transfection efficacy (Fig. 2a, d). Similar patterns were discovered when using C-Ad and co-application of both Ads (Fig. 2b, c and 2e, f). Furthermore, to gain a quantitative insight of the transfection efficiency, levels of SERCA2a and Cx43 protein and mRNA were confirmed by western blotting and q-PCR analysis 48 h after transfection. Fig. 4g, h demonstrated a prominent elevation in SERCA2a or Cx43 protein level both in Ad and Ad + US group compared with the control group. However, we discovered that the protein level of SERCA2a or Cx43 was significantly enhanced in Ad + UTMD group compared to Ad group (Fig. 2g, h). When the S/C-BMBs which carried both S-Ad and C-Ad in a ratio of 1:1 were used, the protein levels of both SERCA2a and Cx43 were declined approximately by 30%. It may be attributed to the decreased loading virus amounts for S-Ad and C-Ad in S/C-BMBs. Intriguingly, we found that the levels of SERCA2a and Cx43 were elevated more prominently in Ad + UTMD group compared to both Ad only and Ad + US group (Fig. 2c, f), indicating that the benefits of UTMD are more pronounced at lower MOI. As expected, the improvement in SERCA2a and Cx43 mRNA levels showed the same pattern with protein in all conditions (Fig. 4i, l). Subsequently, the cell viability of BMSCs in different groups was detected by the experimental setup showed in Fig. S3a. No evident cell damage was found in the UTMD group, with the cell viability remaining at 95.47±2.96%, indicating the ultrasound irradiation (1 W/cm^2, a duty cycle of 20% and a duration of 60 s) was safe for BMSCs (Fig. S3b).

UTMD-mediated co-delivery of S-Ad and C-Ad into infarct zone enhanced SERCA2a and Cx43 expression

Next, we further detected the feasibility of gene co-delivery into the infarct zone of MI rats receiving BMSCs transplantation. Firstly, MI rat model was made (Fig. S4). Electrocardiograms showed that ST-segment typically elevated after LAD ligation. (Fig. S4a, b). Moreover, echocardiography reports a significantly thinning in left ventricular wall and left ventricular dilation 28 d after LAD ligation (Fig. S4c-e). LVEF and LVFS also displayed a significantly reduction after ligation (Fig. S4f). After echocardiography assessment, the heart was harvested, the myocardium of the anterior wall of the left ventricle was pale and collapsed (Fig. S4g). Masson's trichrome staining showed that viable myocardium and scar tissue were identified in red and blue, respectively (Fig. S4h). All of these results showed that the MI model was successfully established. Four weeks after MI, allograft BMSCs were injected directly into the infarct zone and UTMD-mediated localized gene delivery was applied 2 days after this process. Levels of SERCA2a and Cx43 proteins were estimated through immunofluorescence staining at 4 weeks after gene delivery. As presented in Fig. 3a, we observed a drastic reduction in both SERCA2a and Cx43 expression in the infarct zone after MI (control group), and this harsh situation can barely be reversed by BMSCs transplantation (BMSCs group). However, abundant red fluorescence signal representing the expression of SERCA2a was discovered in the B+S+U group, while green fluorescence signal representing the expression of Cx43 was seen in the B+C+U group. Strikingly, both red and green signals, which were more intense compared with the control group, were found in the B+S/C+U group. Western bolt analysis showed that the SERCA2a level in the B+S+U group was approximately 3.83-fold and 4.00-fold higher than that of the control and BMSCs groups (Fig. 3b). Similarly, the Cx43 level in the B+C+U group was approximately 15.50-fold higher than that of the control and BMSCs groups respectively (Fig. 3c). As expected, an obvious enhancement of SERCA2a could be observed in the B+S/C+U group, despite less than that of the B+S+U group. Interestingly, the Cx43 protein level in the B+S/C+U group was even higher than that of the B+C+U group, implicating a connection between SERCA2a and Cx43. Data from ELISA showed the similar pattern with western blotting analysis among groups except for the level of Cx43 in the B+C+U and B+S/C+U groups (Fig. 3d and e).

BMSCs-based gene therapy improves neovascularization in the infarct zone

Given by the fact that the infarcted heart for the late phase of MI undergoes fibrosis and remolding to replace necrotic myocardial cells and eventually led to further deterioration of cardiac function. We evaluated the size of fibrosis via Masson’s trichrome staining at 4 weeks after treatment. No difference of the infarct size was detected among groups according to Fig. 4a and b. Notably, we did observe cardiomyocyte-like cells stained in red within the infract zone in the four groups receiving BMSCs transplantation, except the Control group. In order to confirm this, we further evaluated the expression of myocardial markers in the infarct zone. Results from western blot analysis demonstrated that myocardial ischemia resulted in a robust loss in cTnT (Fig. 4c) and α-actin (Fig. 4d) in the control group. BMSCs transplantation produced the favorable impact on the expression of cTnT and α-actin, with 0.39-fold and 0.23-fold higher than that of the control group, respectively. Remarkably, the expression levels of cTnT and α-actin could be further improved by gene therapy, especially for rats overexpressing Cx43. The cTnT and α-actin levels increased by 1.61-fold and 1.56-fold in the B+S+U group respectively. And in the B+C+U group the increasement was 1.84-fold and 1.95-fold for cTnT and α-actin respectively (Fig. 4c-d).

Since neovascularization is a crucial process in post-MI recovery, we also tested the expression of Factor VIII and VEGF. We evaluated the micro-vessels density (MVD) in the infarct zone by staining the micro-vessels with anti-VIII factor antibody. Immunohistochemical staining assay revealed that MVD enhanced in the BMSCs group compared with the control (Fig. 5a, b). Remarkably, more MVD could be found in the B+C+U and B+S/C+U groups, while overexpression of SERCA2a brought few benefits to neovascularization.

Similarly, strong expression of VEGF was detected in the B+C+U group compared with the others (Fig. 5c), indicating that Cx43 might be beneficial for accelerating neovascularization. Thus, BMSCs in combination with Cx43 overexpression can effectively improve the microenvironment in the infarct region, which might directly contribute to sustain the remaining cardiomyocytes.

BMSCs-based gene therapy recovers ischemic cardiac mechano-electrical function

Since BMSCs-based gene therapy can bring with the beneficial structural changes, we further evaluated the functional alterations 4 weeks after treatment through detecting their contractile and electrophysiological properties. Firstly, echocardiographic assessment was applied to record the LVEF and LVFS, which were critical for cardiac functional parameters. As Fig. 6a exhibited, hypokinesia in the anterior wall and the left ventricle dilation were observed, accompanied by a decrease in LVEF and LVFS post-MI (Fig. 6b, c). Two weeks after BMSCs-based gene therapy, LVEF and LVFS significantly increased both in the B+S+C (34.6±3.13% and 17.3±1.42%) and B+S/C+U groups (35.8±3.31% and 20.5±4.55%). These tendencies maintained until 4 weeks. By contrast, no significant increasements in LVEF and LVFS were discovered in the BMSCs and B+C+U groups compared with the control group, indicating that BMSCs transplantation alone or combined with Cx43 overexpression cannot restore myocardial contractility. Next, rats were subjected to steady-state pacing at progressively faster rating up to 8.0 Hz or the induction of ventricular tachycardia (VT) / ventricular fibrillation (VF) (Fig. 6d). Fig. 6e showed that none of the rats in the SHAM group exhibited pacing-induced VT/VF when the stimulating voltage was set as 7 volts, while 8 (100%) and 7 (87.5%) of the rats in the control and BMSCs groups were susceptible to VT/VF, indicating that BMSCs transplantation brought little profits to electrical stability of myocardium. In contrast, VT/VF propensity was suppressed to around 62.5% in the B+S+U group and 0% in the B+C+U and B+S/C+U groups. Interestingly, VT/VF propensity could still be diminished from 100% to around 50% in the B+C+U and B+S/C+U groups even if we switched the stimulating voltage to 8 volts, revealing that the protective effect of SERCA2a disappeared (Fig. 6f). Thus, our data strongly supported the strategy of localized co-delivery of SERCA2a and Cx43 genes combined with BMSCs can restore rat's ischemic cardiac mechano-electrical functions.

Biosafety assay

Finally, we tested the biocompatibility of BMSCs-based gene therapy *in vivo*. All the measured blood parameters of liver and kidneys from rats on the 15^{th} day post-injection with gene-loaded BMBs fluctuated within the normal ranges, showing no distinct differences compared with the control group

(Fig. Sc-f). Furthermore, H&E staining images of the primary organs, such as the lungs, liver, spleen and kidneys, demonstrated no apparent injury or inflammation in the groups with BMSCs-based gene therapy and control group, as Fig. S3g showed.

Discussion

Despite the multifunction properties of BMSCs, their effect in enhancing cardiac function after MI is still controversial [5] To date, few studies clarified the impact of regenerative method on electrophysiological properties in the failing heart after MI. Above conclusions indicate that BMSCs transplantation alone is not enough to recover the mechano-electrical function of damaged heart. It is necessary to combine the stem cell-based approach with other intervention strategies to improve the efficacy for MI treatment. According to the previous studies, overexpression of some critical genes can improve the function of abnormal cardiomyocytes. Cutler and his collages successfully ameliorate the cardiac function of failing heart through overexpressing SERCA2a gene with AVV9 [33]. Another study indicates that elevation of SERCA2a protein level increases contractile properties of cultured rat cardiomyocytes and significantly improves ventricular function in mice with heart failure [34]. Also, Roell [35] displayed that overexpression of Cx43 markedly reduces post-infarction VT and emphasizes the concept of non-myocyte electrical conduction as a key target in post-infarction cardio protection [35]. In this context, we proposed a strategy that combine stem cell transplantation and site-specific dual gene therapy, which is mediated by UTMD. The current study demonstrates that stem cell-based site-specific dual gene therapy can effectively improve cardiac function and reduce the post-infarct scar-related arrhythmias.

An appropriate vector is the basis to manage a site-specific gene delivery. Although viral vectors were highlighted by their satisfactory transfection efficiency, lack of tissue targeted ability limit the administration route of viral vectors to local injection, which might cause tissue damage. Previous studies have proved that a tissue targeted effective gene transfection could be achieved through binding viral vectors to the surface of MBs with the aid of ultrasound irradiation [36,37]. In our latest research, we also demonstrated that ultrasound beam could destroy the virus loading MBs, release the viral vectors at ventricular level, and realize the tissue targeted gene delivery [22]. In the current study, the resulting BMBs had a micro-scale size (around 1 μm) and showed a good stability. Moreover, these BMBs could produce a clear and stable contrast signal both *in vitro* and *in vivo*, making it possible to monitor the gene delivery progress by ultrasound in a real-time manner. Most importantly, BMBs showed an ideal gene loading capacity that above 90%, just as proved by flow cytometry and qPCR analysis.

In our study, we validated *in vitro* that UTMD could release the Ad from BMBs and improve the gene transfection efficiency. Images of fluorescent microscope clearly presents that Ad itself possess a relatively high transfection efficiency. However, compared with the cells received UTMD, more cells expressing fluorescent protein could be observed, strongly indicating that UTMD helps more virus encoding fluorescent protein gene enter cytoplasm by making transient pore on cell membrane [38]. Interestingly, during the *in vitro* experiment we found that the effect of UTMD was more prominent when the MOI was lower, indicating the effect of UTMD was underestimated, and we hypothesis that a

reasonable combination of MOI and UTMD might significantly decrease the amounts of viral vectors when achieving an ideal transfection efficiency.

As demonstrated by the immunofluorescence detection in MI rat model, the level of SERCA2a and Cx43 was sharply decreased so much in infarct zone of MI rats that we can hardly found fluorescence signals, strongly indicating that gene expressions of SERCA2a and Cx43 failed due to the myocardial ischemic stress [7]. A reasonable explanation is that it's not only the loss of cardiomyocytes but also the absence of crucial protein that induced post-MI heart failure and arrhythmias. Our results also illustrated that the level of SERCA2a and Cx43 in the infarct zone cannot be reversed by only BMSCs transplantation. Thus, cell-based intervention was not enough to regain mechano-electrical function of damaged heart. Fortunately, the level of SERCA2a and Cx43 showed a considerable elevation through UTMD-mediated dual gene co-delivery. By contrast, the expression of SERCA2a presented a robust increase in B+S+U group, while level of Cx43 did not show any improvement. Similarly, B+C+U group only showed a promotion in Cx43 expression but not in SERCA2a, implying that there was no obvious correlation between these two proteins.

It has been well elucidated that rat BMSCs can secrete paracrine factors including VEGF-1 to trigger angiogenic and migratory effects at the site of the infarct to promote myocardial healing and to improve the cardiac function [39]. In the current study, we also found that the level of VEGF and MVD in the infarct zone had a significant increasement after BMSCs transplantation, indicating that paracrine effect plays an essential role in BMSCs tissue repair and angiogenesis. Notably, our results revealed that overexpression of Cx43 upgraded the angiogenesis effect by BMSCs, while overexpression of SERCA2a brought no interest to local VEGF level. With these data, we assume that overexpression of Cx43 can improve the microenvironment of infarct area by promote the level of VEGF. Indeed, more cardiomyocyte-like cells and higher level of myocardial markers in the infarct zone were detected among the groups with BMSCs transplantation. Although we cannot identify the origin of these cells, we can speculate that BMSCs in combination with Cx43 will significantly relive the harsh conditions within the infarct zone and help to rejuvenate cardiac function.

Myocardial contractility and electrical stability of myocardium are two most critical evaluation indexes for cardiac function. In the current study, we applied echocardiography and ECG to record the alteration of cardiac function in each group after treatment. From the results of echocardiography, we can see that ischemia brings a disastrous blow upon systolic function, which was manifested by plummeting LVEF. Moreover, arrhythmias could be induced very easily in MI rats by steady-state pacing, which indicates a poor electrical stability of myocardium. Furthermore, as revealed by our results, rats received BMSCs transplantation alone do not show any solid signs of recovery both in myocardial contractility and electrical stability. Until now, we can deduce that the effect of BMSCs transplantation in cardiac function recovery is limited. However, gene therapy combined with cell transplantation can bring with encouraging news. Echocardiography clearly showed that ventricular wall motion of those rats received SERCA2a transfection was significantly improved, indicating the essential role of SERCA2a in maintaining mechanical function of myocardium [33,40]. Moreover, we also discovered that rats treated with

SERCA2a showed a better resistance to pacing induced arrhythmias than MI group, but this virtue of SERCA2a overexpression vanished when we turn up the voltage, indicating a limited effect of SERCA2a in restoring electrophysiological properties. In particular, we revealed that overexpression of Cx43 in MI heart could effectively suppress pacing induced arrhythmias, but did nothing to restore myocardial contractility. Based on these findings, we surmised that there were no interactions between SERCA2a and Cx43 [8], and overexpression of neither of them solely could meet our goal. Guided by these findings above, we applied two genes together after BMSCs transplantation. Remarkably, rats receiving dual-gene therapy showed an intrinsic improvement both in myocardial contractility and electrophysiological properties, highlighting the necessity for rebuild the gene network in damaged heart rather than the supplement of a single particular gene [41].

Conclusions

the findings in the present study, together with the published studies from our own laboratory and from other research group, came to the following conclusions: 1) UTMD is a reliable tool to realize site-specific gene delivery, and in the current study, we managed to deliver two genes in one administration; 2) BMSCs transplantation can improve the microenvironment of infract zone, however it does few to restore cardiac function; 3) Cell-based dual gene therapy solidly ameliorates myocardial contractility and electrophysiological properties, emphasizing the necessity for rebuild the gene network in a damaged heart rather than the supplement of a single gene. 4) BMSCs transplantation combined with localized dual-gene co-delivery by UTMD might point out a novel strategy to recover mechano-electrical function of ischemic heart.

Abbreviations

BMSCs: bone marrow mesenchymal stem cells; MI: myocardial infarct; VEGF: vascular endothelial growth factor; SDF-1: stromal cell derived factor 1; HGF: hepatocyte growth factor; CXCR4: CXC chemokine receptor 4; SERCA2a: Ca2+-ATPase 2a; Cx43: Connexin 43; SR: sarcoplasmic reticulum; GJs: gap junctions; Ad: adenovirus; AAV: adeno associated virus; UTMD: ultrasound targeted microbubble destruction; BMBs: biotinylated microbubbles; S-Ad: FITC-labeled SERCA2a adenovirus; C-Ad: rhodamine-labeled Cx43 adenovirus; S-BMBs: SERCA2a-Ad-BMBs; C-BMBs: Cx43-Ad-BMBs; S/C-BMBs: SERCA2a-Ad/Cx43-Ad-BMBs; SD: Sprague Dawley; US: ultrasound; MOI: multiplicity of infection; CCK-8: Counting Kit-8; LAD: left anterior descending artery; LVEF: left ventricle ejection fraction; LVFS: left ventricle fractional shortening; SEM: scanning electronic microscopy; MVD: micro-vessels density; VT: ventricular tachycardia; VF: ventricular fibrillation.

Declarations

Acknowledgements

We thank Drs. Taosheng Li, Department of Stem Cell Biology, Atomic Bomb Disease Institute, Nagasaki University, Nagasaki 852-8523, Japan. We also thank Rongjun Guo, Yu Su in the Experimental Animal Center of Shenzhen Institute of Synthetic Biology for their technical assistance.

Authors' contributions

YM-M, FY, and LN-G have substantial contributions to the conception or design of the work; WW and BT contributed to the data collection, analysis and interpretation; WW did the data; WW and BT drafted the manuscript; YM-M, and FY contributed to the critical revision of the manuscript. All authors read and approved the final manuscript.

Funding

This work was supported by National Natural Science Foundation of China [8166070043, 81871376], Regional Cooperative Innovation Program of Autonomous Region (Science and Technology Aid Xinjiang Program) [Grant No.2018E02062], Guangdong Innovation Platform of Translational Research for Cerebrovascular Diseases, and Shenzhen Science and Technology Innovation Committee [Grant No. JCYJ20180507182420114, ZDSYS201802061806314].

Availability of data and materials

The datasets generated during and/or analyzed during the current study are available from the corresponding author on reasonable request.

All data generated or analyzed during this study are included in this published article (and its supplementary information files).

The datasets generated during and/or analyzed during the current study are not publicly available due to reason(s) why data are not public but are available from the corresponding author on reasonable request.

Ethics approval and consent to participate

The experimental protocol was approved by the Animal Ethics Committee of the First Affiliated Hospital of Xinjiang Medical University (approval number of IACUC-20160218-057).

Consent for publication

Not applicable.

Competing interests

The authors declare that they have no conflict of interest.

Author details

[1] Department of Echocardiography, Xinjiang Medical University Affiliated First Hospital, Urumqi, 830011, China.

[2] CAS Key Laboratory of Quantitative Engineering Biology, Shenzhen Institute of Synthetic Biology, Shenzhen Institutes of Advanced Technology, Chinese Academy of Sciences, Shenzhen, 518055, China.

References

1. Benjamin EJ, P Muntner, A Alonso, MS Bittencourt, CW Callaway, AP Carson, AM Chamberlain, AR Chang, S Cheng, SR Das, et al. Heart Disease and Stroke Statistics-2019 Update: A Report From the American Heart Association. Circulation 2019; 139:e56-e528.
2. Miao C, M Lei, W Hu, S Han and Q Wang. A brief review: the therapeutic potential of bone marrow mesenchymal stem cells in myocardial infarction. Stem Cell Res Ther 2017; 8:242.
3. Gieseke F, A Kruchen, N Tzaribachev, F Bentzien, M Dominici and I Müller. Proinflammatory stimuli induce galectin-9 in human mesenchymal stromal cells to suppress T-cell proliferation. Eur J Immunol 2013; 43:2741-9.
4. Ebelt H, M Jungblut, Y Zhang, T Kubin, S Kostin, A Technau, S Oustanina, S Niebrügge, J Lehmann, K Werdan and T Braun. Cellular cardiomyoplasty: improvement of left ventricular function correlates with the release of cardioactive cytokines. Stem Cells 2007; 25:236-44.
5. Li X, H Zhao, C Qi, Y Zeng, F Xu and Y Du. Direct intercellular communications dominate the interaction between adipose-derived MSCs and myofibroblasts against cardiac fibrosis. Protein Cell 2015; 6:735-45.
6. Ikhapoh IA, CJ Pelham and DK Agrawal. Atherogenic Cytokines Regulate VEGF-A-Induced Differentiation of Bone Marrow-Derived Mesenchymal Stem Cells into Endothelial Cells. Stem Cells Int 2015; 2015:498328.
7. Renaud-Gabardos E, F Tatin, F Hantelys, B Lebas, D Calise, O Kunduzova, B Masri, F Pujol, P Sicard, P Valet, J Roncalli, X Chaufour, B Garmy-Susini, A Parini and AC Prats. Therapeutic Benefit and Gene Network Regulation by Combined Gene Transfer of Apelin, FGF2, and SERCA2a into Ischemic Heart. Mol Ther 2018; 26:902-916.
8. Motloch LJ, M Cacheux, K Ishikawa, C Xie, J Hu, J Aguero, KM Fish, RJ Hajjar and FG Akar. Primary Effect of SERCA 2a Gene Transfer on Conduction Reserve in Chronic Myocardial Infarction. J Am Heart Assoc 2018; 7:e009598.
9. Igarashi T, JE Finet, A Takeuchi, Y Fujino, M Strom, ID Greener, DS Rosenbaum and JK Donahue. Connexin gene transfer preserves conduction velocity and prevents atrial fibrillation. Circulation 2012; 125:216-25.
10. Gorski PA, SP Jang, D Jeong, A Lee, P Lee, JG Oh, V Chepurko, DK Yang, TH Kwak, SH Eom, ZY Park, YJ Yoo, DH Kim, H Kook, Y Sunagawa, T Morimoto, K Hasegawa, J Sadoshima, P Vangheluwe, RJ Hajjar, WJ Park and C Kho. Role of SIRT1 in Modulating Acetylation of the Sarco-Endoplasmic Reticulum Ca(2+)-ATPase in Heart Failure. Circ Res 2019; 124:e63-e80.

11. Zhang P, C Toyoshima, K Yonekura, NM Green and DL Stokes. Structure of the calcium pump from sarcoplasmic reticulum at 8-A resolution. Nature 1998; 392:835-9.
12. Chelu MG and N Li. "Sorting" SERCA2a: A novel therapeutic strategy in heart failure? Int J Cardiol 2018; 272:306-307.
13. Nielsen MS, LN Axelsen, PL Sorgen, V Verma, M Delmar and NH Holstein-Rathlou. Gap junctions. Compr Physiol 2012; 2:1981-2035.
14. Michela P, V Velia, P Aldo and P Ada. Role of connexin 43 in cardiovascular diseases. Eur J Pharmacol 2015; 768:71-6.
15. Dunbar CE, KA High, JK Joung, DB Kohn, K Ozawa and M Sadelain. Gene therapy comes of age. Science 2018; 359.
16. Zhang X, X Zhang, S Hu, M Zheng, J Zhang, J Zhao, X Zhang, B Yan, L Jia, J Zhao, K Wu, A Yang and R Zhang. Identification of miRNA-7 by genome-wide analysis as a critical sensitizer for TRAIL-induced apoptosis in glioblastoma cells. Nucleic Acids Res 2017; 45:5930-5944.
17. Ishikawa K, T Weber and RJ Hajjar. Human Cardiac Gene Therapy. Circ Res 2018; 123:601-613.
18. Saraiva J, RJ Nobre and L Pereira de Almeida. Gene therapy for the CNS using AAVs: The impact of systemic delivery by AAV9. J Control Release 2016; 241:94-109.
19. Lukashev AN and AA Zamyatnin, Jr. Viral Vectors for Gene Therapy: Current State and Clinical Perspectives. Biochemistry (Mosc) 2016; 81:700-8.
20. Zhang L, Z Sun, P Ren, M You, J Zhang, L Fang, J Wang, Y Chen, F Yan, H Zheng and M Xie. Localized Delivery of shRNA against PHD2 Protects the Heart from Acute Myocardial Infarction through Ultrasound-Targeted Cationic Microbubble Destruction. Theranostics 2017; 7:51-66.
21. Fujii H, Z Sun, SH Li, J Wu, S Fazel, RD Weisel, H Rakowski, J Lindner and RK Li. Ultrasound-targeted gene delivery induces angiogenesis after a myocardial infarction in mice. JACC Cardiovasc Imaging 2009; 2:869-79.
22. Yang L, F Yan, J Ma, J Zhang, L Liu, L Guan, H Zheng, T Li, D Liang and Y Mu. Ultrasound-Targeted Microbubble Destruction-Mediated Co-Delivery of Cxcl12 (Sdf-1alpha) and Bmp2 Genes for Myocardial Repair. J Biomed Nanotechnol 2019; 15:1299-1312.
23. Liu HL, CH Fan, CY Ting and CK Yeh. Combining microbubbles and ultrasound for drug delivery to brain tumors: current progress and overview. Theranostics 2014; 4:432-44.
24. Yan F, X Li, Q Jin, J Chen, R Shandas, J Wu, L Li, T Ling, W Yang, Y Chen, X Liu and H Zheng. Ultrasonic imaging of endothelial CD81 expression using CD81-targeted contrast agents in in vitro and in vivo studies. Ultrasound Med Biol 2012; 38:670-80.
25. Kilkenny C, WJ Browne, IC Cuthill, M Emerson and DG Altman. Improving bioscience research reporting: the ARRIVE guidelines for reporting animal research. PLoS Biol 2010; 8:e1000412.
26. Kirihara Y, M Takechi, K Kurosaki, Y Kobayashi and T Kurosawa. Anesthetic effects of a mixture of medetomidine, midazolam and butorphanol in two strains of mice. Exp Anim 2013; 62:173-80.

27. Hou Y, C Huang, X Cai, J Zhao and W Guo. Improvements in the establishment of a rat myocardial infarction model. J Int Med Res 2011; 39:1284-92.
28. Su G, L Liu, L Yang, Y Mu and L Guan. Homing of endogenous bone marrow mesenchymal stem cells to rat infarcted myocardium via ultrasound-mediated recombinant SDF-1alpha adenovirus in microbubbles. Oncotarget 2018; 9:477-487.
29. Wang G, Y Bi, T Ye, Q Zhang and M Wei. Resveratrol exerts anti-arrhythmic effects in rats with myocardial infarction through up-regulation of cardiac connexin43 expression. Chin J Cardiac Arrhyth 2016; 20:236-240.
30. Milkiewicz M, CW Pugh and S Egginton. Inhibition of endogenous HIF inactivation induces angiogenesis in ischaemic skeletal muscles of mice. J Physiol 2004; 560:21-6.
31. Lyakhov I, R Zielinski, M Kuban, G Kramer-Marek, R Fisher, O Chertov, L Bindu and J Capala. HER2- and EGFR-specific affiprobes: novel recombinant optical probes for cell imaging. Chembiochem 2010; 11:345-50.
32. Lu J, YY Yao, QM Dai, GS Ma, SF Zhang, L Cao, LQ Ren and NF Liu. Erythropoietin attenuates cardiac dysfunction by increasing myocardial angiogenesis and inhibiting interstitial fibrosis in diabetic rats. Cardiovasc Diabetol 2012; 11:105.
33. Cutler MJ, X Wan, BN Plummer, H Liu, I Deschenes, KR Laurita, RJ Hajjar and DS Rosenbaum. Targeted sarcoplasmic reticulum Ca2+ ATPase 2a gene delivery to restore electrical stability in the failing heart. Circulation 2012; 126:2095-104.
34. Kho C, A Lee, D Jeong, JG Oh, PA Gorski, K Fish, R Sanchez, RJ DeVita, G Christensen, R Dahl and RJ Hajjar. Small-molecule activation of SERCA2a SUMOylation for the treatment of heart failure. Nat Commun 2015; 6:7229.
35. Roell W, AM Klein, M Breitbach, TS Becker, A Parikh, J Lee, K Zimmermann, S Reining, B Gabris, A Ottersbach, R Doran, B Engelbrecht, M Schiffer, K Kimura, P Freitag, E Carls, C Geisen, GD Duerr, P Sasse, A Welz, A Pfeifer, G Salama, M Kotlikoff and BK Fleischmann. Overexpression of Cx43 in cells of the myocardial scar: Correction of post-infarct arrhythmias through heterotypic cell-cell coupling. Sci Rep 2018; 8:7145.
36. Bazan-Peregrino M, B Rifai, RC Carlisle, J Choi, CD Arvanitis, LW Seymour and CC Coussios. Cavitation-enhanced delivery of a replicating oncolytic adenovirus to tumors using focused ultrasound. J Control Release 2013; 169:40-7.
37. Sorace AG, JM Warram, M Mahoney, KR Zinn and K Hoyt. Enhancement of adenovirus delivery after ultrasound-stimulated therapy in a cancer model. Ultrasound Med Biol 2013; 39:2374-81.
38. Yu J, Z Chen and F Yan. Advances in mechanism studies on ultrasonic gene delivery at cellular level. Prog Biophys Mol Biol 2019; 142:1-9.
39. Selvasandran K, G Makhoul, PK Jaiswal, R Jurakhan, L Li, K Ridwan and R Cecere. A Tumor Necrosis Factor-alpha and Hypoxia-Induced Secretome Therapy for Myocardial Repair. Ann Thorac Surg 2018; 105:715-723.
40. Braunwald E. The war against heart failure: the Lancet lecture. Lancet 2015; 385:812-24.

41. Drozdov I, A Didangelos, X Yin, A Zampetaki, M Abonnenc, C Murdoch, M Zhang, CA Ouzounis, M Mayr, S Tsoka and AM Shah. Gene network and proteomic analyses of cardiac responses to pathological and physiological stress. Circ Cardiovasc Genet 2013; 6:588-97.

Tables

Table 1 The Characteristics of BMBs.

	Average diameter (μm)	Concentration (10^9/ml)	PdI
BMBs	1.10 ± 0.65	4.63 ± 0.62	0.26±0.05
S-BMBs	1.19 ± 0.28*	0.87 ± 0.02*	0.15±0.02*
C-BMBs	1.18 ± 0.16*	0.83 ± 0.08*	0.16±0.01*
S/C-BMBs	1.21 ± 0.22*	0.91 ± 0.04*	0.15±0.02*

Note: C-BMBs: Cx43-Ad-BMBs; S-BMBs: SERCA2a-Ad-BMBs; S/C-BMBs: SERCA2a-Ad/Cx43-Ad-BMBs. *: compared with BMBs group P 0.05.

Figures

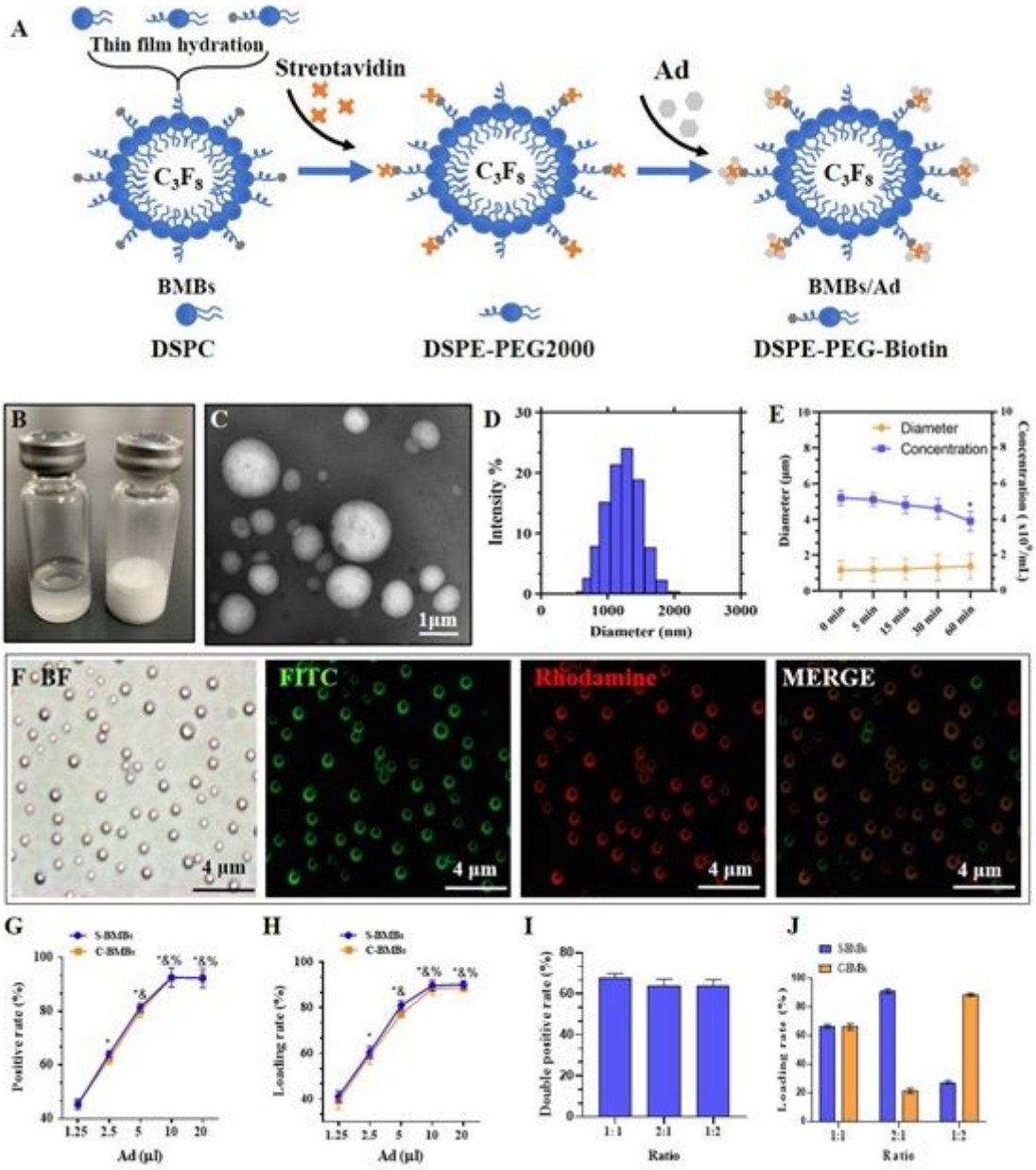

Figure 1

Fabrication and characterization of Ad loaded BMBs. (a) Schematic diagram of preparation of BMBs and Ad-loading BMBs (Ad-BMBs). (b) Photograph of BMBs solution before (transparent) and after (milky) oscillation. (c) SEM image of BMBs. Scale bar=1μm. (d) Size distribution of BMBs by Zeta Sizer Nano. (e) Stability of BMBs manifested by diameter and concentration. N=6/time point, *compared with 0 min, $P < 0.05$. (f) Bright-field and the corresponding fluorescent images of Ad-BMBs. Scale bar=10 μm. (g-h) Positive rate and gene-loading rate of Ad-BMBs with different dose of Ad by flow cytometry and qPCR (n=6/ concentration). *compared with 1.25 μl $P < 0.05$, &compared with 2.5 μl $P < 0.05$, %compared with 5 μl, $P < 0.05$. (i-j) Dual-gene loading capacity of BMBs with different S-Ad to C-Ad ratio. N=6/group, *$P < 0.05$. C: Cx43; S: SERCA2a.

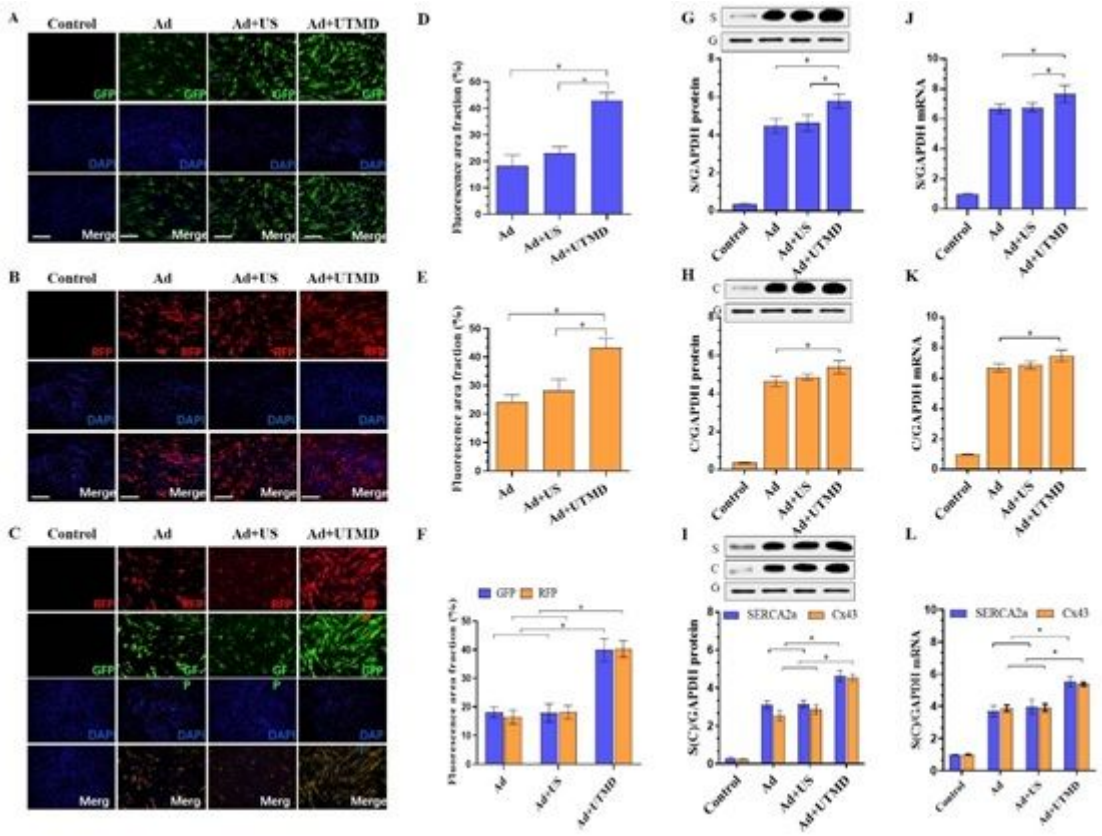

Figure 2

Detection of gene expression after UTMD-mediated gene transfection in Vitro. (a-c) Gene transfection detected by fluorescence microscope. Scale bar=100 μm. (d-f) Fluorescence area fraction of the GFP, RFP and both. N=3/group, *P < 0.05. (g-i) The protein levels of SERCA2a, Cx43 and both by WB. N=3/group, 1×106 cells/group, *P < 0.05. (j-l) The mRNA levels of SERCA2a, Cx43 and both by q-PCR. N=3/group, 1×106 cells/group,*P < 0.05.

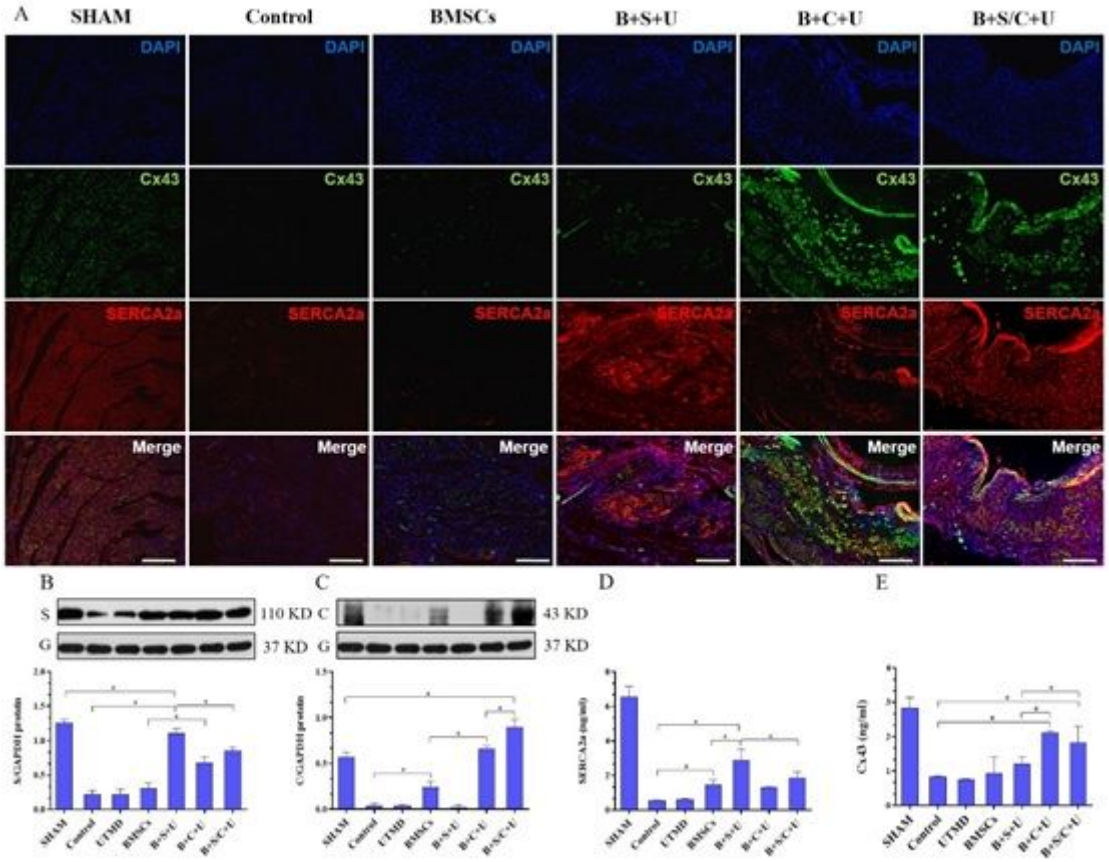

Figure 3

Detection of the levels of SERCA2a and Cx43 Proteins. (a) Immunofluorescence in the infarct zone 4 weeks after BMSCs-based gene therapy. Scale bar=260 μm. (b-c) Detection of the SERCA2a and Cx43 levels by WB. N=3/group, *P<0.05. (d-e) Detection of the SERCA2a and Cx43 levels by ELISA. N=3/group, NS=Non significance, *P<0.05. B: BMSCs; C: Cx43; G: GAPDH; S: SERCA2a; U: UTMD.

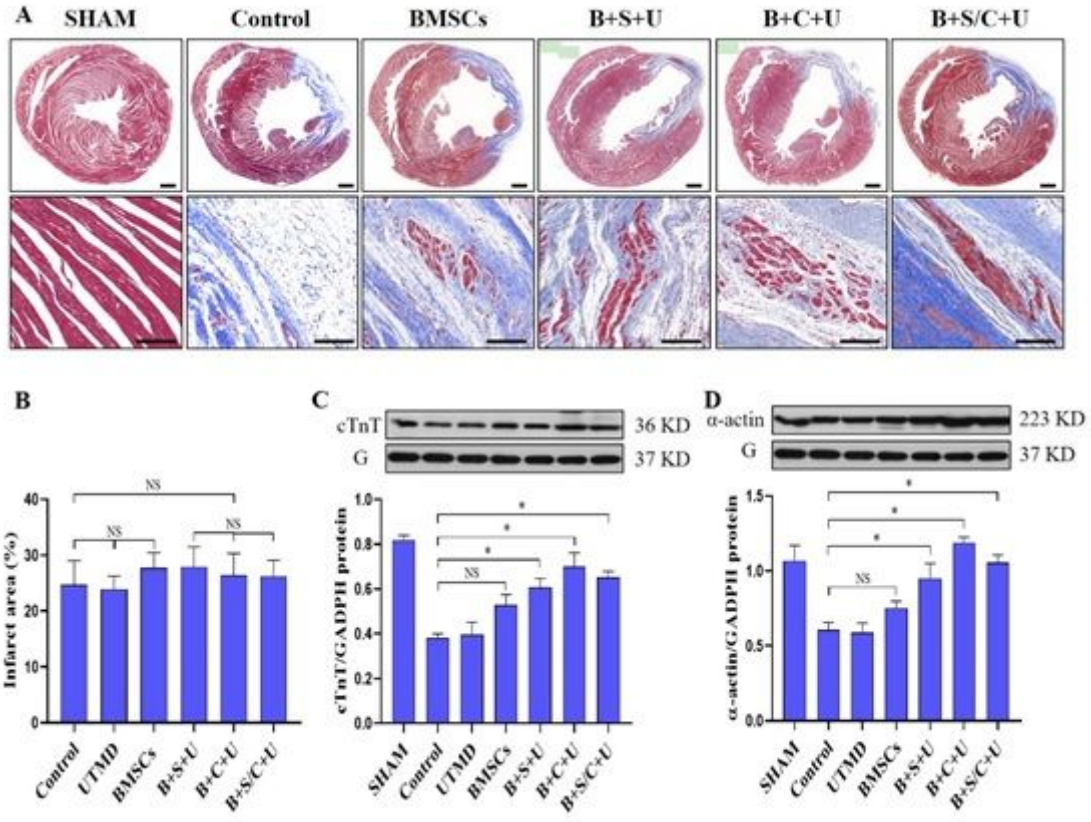

Figure 4

Evaluation of infarct size and the level of myocardial markers in the infarct zone. (a) Representative images of Masson's staining, scale bar = 1000μm/50μm. (b) Quantitative data of the infarcted zone. Data is expressed as a percentage of infarcted area (blue) with the total area of heart tissues of left ventricle. NS=Non significance. (c-d) Detection of cTnT and α-actin level by WB analysis. N=3/group, *P<0.05. B: BMSCs; C: Cx43; G: GAPDH; S: SERCA2a; U: UTMD.

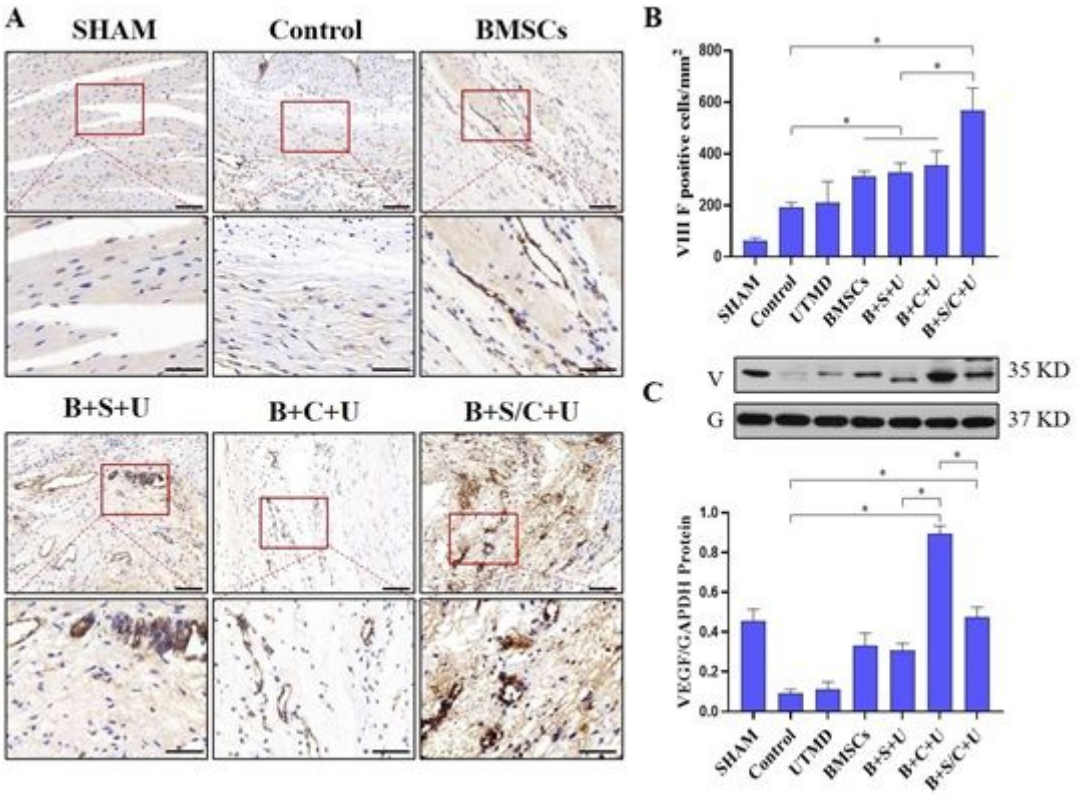

Figure 5

Detection of neovascularization in the infarct zone. (a) Representative images of immunohistochemical staining with anti-Ⅷ factor antibody in the infarct area, Scale bar = 90 μm/50 μm (zoom). (b) Quantitative data of the MVD positively stained with Ⅷ-factor antibody. N=3/group, NS = Non significance, *P<0.05. (c) Evaluation of VEGF level in the infarct zone, *P<0.05. B: BMSCs; C: Cx43; G: GAPDH; MVD: micro-vessels density; S: SERCA2a; S: SERCA2a; U: UTMD.

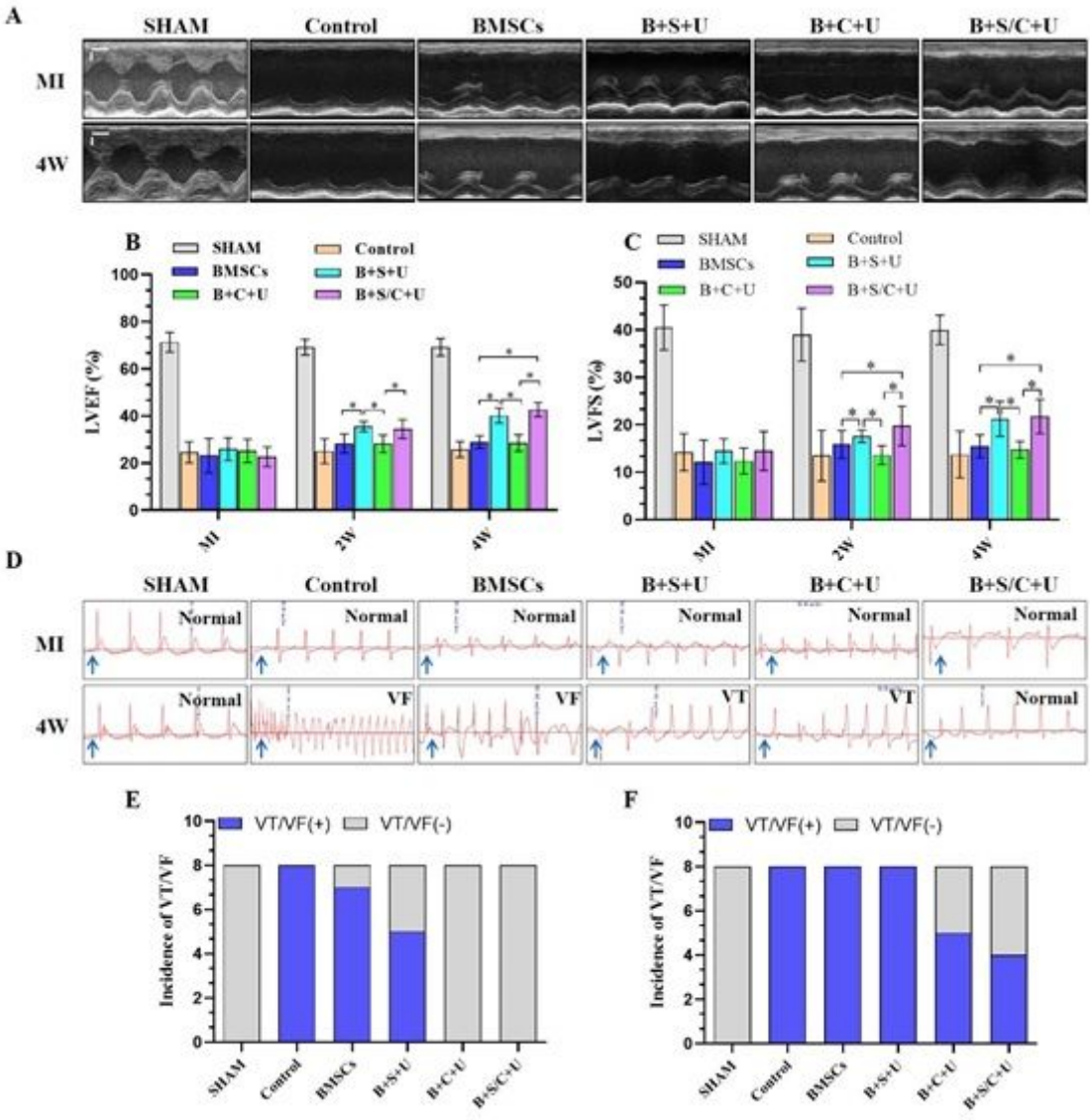

Figure 6

Evaluation of mechano-electrical function. (a) Representative images of M-mode echocardiography. (b-c) Evaluation of LVEF and LVFS at 2-week and 4-week post-intervention. N=8/group, NS = Non significance, *P<0.05. (d) Representative images of electrocardiogram. (e-f) Incidence of VT/VF after steady-state pacing at 4-week post-intervention when the voltage was set as 7 and 8 respectively. N=8. B: BMSCs; C: Cx43; S: SERCA2a; U: UTMD.

Supplementary Files

This is a list of supplementary files associated with this preprint. Click to download.

- SupplementaryMaterial.docx
- gb.JPG